Failure analysis of adhesively bonded joints in crash simulations

R. Mahnken, M. Hentrich

Chair of Engineering Mechanics (LTM), University of Paderborn
rolf.mahnken@ltm.upb.de

Abstract: Experimental evidence of certain adhesive materials reveals a hardening regime with a pronounced strength difference between tension, torsion or combined loading. The results for the stress-strain curves are strongly rate dependent. Additionally a softening regime is observed, also dependent on the stress state of tension, torsion or combined loading. For simulation of these phenomena a Perzyna type flow parameter is introduced, It is formulated on the basis of an overstress function dependent on the first and second basic invariants of the related effective stress tensor. A plastic potential with the same mathematical structure is introduced to obtain the evolution equation of the inelastic strains. The numerical implementation for the case of rate dependency is explained in detail and its capability is verified on the basis of experimental data for rate dependency. Furthermore, the constitutive equations of rate dependency are extended to softening behavior. This approach is used in a second example to investigate failure of an adhesively bonded joint in a double-U-spape specimen.

Keywords: Constitutive Model, Plasticity, Damage, Experimental Verification

1. Introduction

Adhesion has gained growing application areas for the bonding process in the industrial field in recent years. Examples for applications are the industrial branches of automotive industry, the aeroplane construction and the building industry. There are several aspects, which make the adhesion process advantageous to other bonding processes: 1.) Adhesion has favourable properties for automation. 2.) The adhesive is able to make seams tight where otherwise an additional sealing would be necessary. 3.) Structural adhesive bonds in vehicle construction permit a stiffness increase of the car body as well as an improved crash performance at a nearly constant weight. 4.) The adhesion technique offers ideal features for mixed constructions.

This publication is related to the group of so-called crash optimized adhesives. Experimental observations of this material, basically show the following characteristics

1. There is a pronounced nonlinear regime, which is dependent on the tension-torsion relation. In particular the yield strength is largest for pure tension and smallest for pure torsion thus resulting into a *strength difference effect* (SD-effect), Schlimmer (2003).
2. Following a hardening regime a *softening* regime follows in the stress strain relations.
3. The stress-strain behaviour is strongly *rate dependent*, Disse (2004)

Several publications can be found in the literature for simulation of inelastic material behaviour with strength difference effects. Many of the approaches are based on a stress potential dependent on the stress tensor and further state variables, which describe e.g. the state of hardening, softening or damage, respectively. Typically, the potential is formulated with polynomials in terms of invariants of the related stress tensor. One of the earlier formulations of this type is given by Schlimmer (1974). Along this line further constitutive equations have been formulated e.g. in Zolochoskii (1989), Altenbach *et al* (1995), Ehlers (1995), Betten *et al.* (1998), Mahnken (2001) amongst others.

As an extension to the presentation of Mahnken and Schlimmer (2005) we are concerned with the simulation of rate dependent properties and softening behaviour of adhesive materials. To this end rate dependent constitutive equations are introduced consisting of a Perzyna type plastic parameter. This is formulated in terms of an overstress function dependent on the first invariant of the stress tensor and the second invariant of the deviatoric stress tensor according to Schlimmer (1974). Additionally a plastic potential with the same mathematical structure is introduced to formulate the evolution equation for the inelastic strains. Two different approaches (referred as “Case 1” and “Case 2” in Mahnken and Schlimmer (2005)) are postulated for evolution of a strain like internal variable. Upon considering thermodynamic consistency of the model equations, for both Case 1 and Case 2 some restrictions on the material parameters are derived. Furthermore, Case 2 gives a restriction on evolution of the strain like internal variable.

Different concepts are known from the literature for simulation of softening. Two well known approaches are published in Gurson (1977) and Lemaitre (1996). The first approach activates softening under a pure volumetric stress mode, thus rendering the material undamaged for a stress mode in shear. The second approach activates softening under a pure stress mode in shear, thus rendering the material undamaged for a volumetric stress mode. Both approaches have in common, that additional evolution equations are introduced for softening representation. Additional approaches to simulate softening and failure are described in Dean *et al.* (2004), Duncan and Dean (2004). In this work we propose a simple approach which accounts for both, softening evolution subject to deviatoric and volumetric stress states.

An extensive part of the paper is devoted to numerical aspects. An implicit Euler backward scheme is used for integration of the evolution equations for rate dependency, thus resulting into a (local) nonlinear multi dimensional problem. It is shown, that this problem can be reduced to an equivalent one-dimensional problem for Case 2, whereas the dimension for Case 1 is two. The resulting nonlinear equation is solved with a Newton algorithm. Additionally the corresponding algorithmic tangent operator for the (global) equilibrium iteration of the finite element structure scheme is derived. The constitutive equations are implemented as a UMAT subroutine for ABAQUS and are combined with the adhesive finite element COH3D8 of ABAQUS.

An outline of this work is as follows: Section 2 considers the constitutive equations to simulate rate dependent material behaviour coupled to the SD effect of adhesive materials. To this end an overstress function and a plastic potential are introduced in order to formulate the evolution equation for the inelastic strains. Furthermore consequences of thermodynamic consistency are investigated. Section 3 describes the integration scheme and the implementation into a finite element program for rate dependent plasticity. An example illustrates the performance of the model to simulate rate dependent material behaviour coupled to the SD effect, on the basis of experimental data for axial and shear loading. Section 4 summarizes briefly the extension of our model to softening behaviour. This approach is used in a second example to investigate failure of an adhesively bonded joint in a double-U-shape specimen.

Notations: Square brackets [•] are used throughout the paper to denote 'function of' in order to distinguish from mathematical groupings with parenthesis (•). The three *basic invariants* $I_1[\mathbf{A}], I_2[\mathbf{A}], I_3[\mathbf{A}]$ of an arbitrary second order tensor $\mathbf{A}$ are defined as

$$I_1[\mathbf{A}] = 1 : \mathbf{A}, \quad I_2[\mathbf{A}] = \frac{1}{2} 1 : \mathbf{A}^2, \quad I_3[\mathbf{A}] = \frac{1}{3} 1 : \mathbf{A}^3 . \tag{1}$$

Here 1 is a second order unit tensor, defined as $1 \cdot \mathbf{u} = \mathbf{u}$ for arbitrary vector (first order tensor) $\mathbf{u}$. Consequently the deviatoric/volumetric additive decomposition of $\mathbf{A}$ can be written as

$$\mathbf{A} = \mathbf{A}_{dev} + \mathbf{A}_{vol}, \quad \text{where} \quad \mathbf{A}_{dev} = \mathbf{I}_{dev} : \mathbf{A}, \quad \mathbf{A}_{vol} = \frac{1}{3} I_1[\mathbf{A}] 1, \quad \mathbf{I}_{dev} = \mathbf{I} - \frac{1}{3} 1 \otimes 1, \tag{2}$$

and where $\mathbf{I}$ is a fourth order unit tensor, defined as $\mathbf{I} : \mathbf{A} = \mathbf{A}$.

2. Constitutive equations for rate dependent plasticity

2.1 Strain decomposition and Hooke's law

Upon using standard notation within a geometrically linear theory the following relations are valid:

$$\begin{aligned} &1. \quad \boldsymbol{\varepsilon} &&= \boldsymbol{\varepsilon}^{el} + \boldsymbol{\varepsilon}^{pl} \\ &2. \quad \boldsymbol{\varepsilon}^{el} &&= \mathbf{C}^{-1} : \boldsymbol{\sigma} \\ &3. \quad \mathbf{C} &&= 2G\,\mathbf{I}_{dev} + K\,\mathbf{1} \otimes \mathbf{1} \end{aligned} \tag{3}$$

Equation 3.1 expresses the additive decomposition of the total strain tensor $\boldsymbol{\varepsilon}$ into an elastic part $\boldsymbol{\varepsilon}^{el}$ and a plastic part $\boldsymbol{\varepsilon}^{pl}$, and in Equation 3.2 the stress tensor $\boldsymbol{\sigma}$ is related to the elastic strain tensor $\boldsymbol{\varepsilon}^{el}$ by the fourth order elasticity tensor $\mathbf{C}$. For the case of isotropic linear elasticity $\mathbf{C}$ is given in Equation 3.3, where G and K denote the shear and bulk modulus, respectively, and the fourth order projection tensor $\mathbf{I}_{dev}$ is defined in Equation 2. The plastic strain tensor $\boldsymbol{\varepsilon}^{pl}$ of Equation 3.1 is obtained from evolution equations as discussed next.

2.2 Overstress function and plastic potential

An overstress function for an elastic/viscoplastic continuum in terms of the symmetric second order stress tensor $\boldsymbol{\sigma}$ can be written in the form $\Phi(\boldsymbol{\sigma}) = 0$. For an isotropic material the overstress function reduces as $\Phi(I_1, I_2, I_3) = 0$, where the three basic invariants I_1, I_2, I_3 of the Cauchy stress tensor are determined according to Equation 1. Alternatively the overstress function can be recast into the form $\Phi(I_1, I_2^{'}, I_3^{'}) = 0$, where the prime refers to invariants of the deviatoric stress tensor $\boldsymbol{\sigma}_{dev}$, i.e.

$$I_1 = \mathbf{1} : \boldsymbol{\sigma}, \qquad I_2^{'} = \frac{1}{2} \mathbf{1} : \boldsymbol{\sigma}_{dev}^2, \quad I_3^{'} = \frac{1}{3} \mathbf{1} : \boldsymbol{\sigma}_{dev}^3 . \tag{4}$$

As discussed extensively in Schlimmer (1974) and Ehlers (2004) a general overstress function of this type allows simultaneously for the two effects of pressure stress state and deviatoric stress state dependence, where the latter can be different e.g. in tension and compression. However, the experimental observations of these effects require sophisticated and careful measurements techniques. In order to simulate the experimental data currently available for adhesive materials the third invariant $I_3^{'}$ is disregarded thus restricting our attention to the following overstress function:

$$\begin{array}{llcl}
1. & \Phi & = & I_2^{'} - \frac{1}{3}\varphi \\
2. & \varphi & = & Y^2 - a_1 Y_0 I_1 - a_2 I_1^2 \\
3. & Y & = & Y_0 + R(e_v) \\
4. & R(e_v) & = & q(1 - \exp(-b e_v)) + H e_v
\end{array} \tag{5}$$

Remarks:

1. The above overstress function has basically the mathematical structure formulated by Schlimmer (1974). Let us recall from Ehlers (1995) that it reduces to certain well-known criteria. Then for the case $a_1 = a_2 = 0$ the von Mises cylinder is obtained. For $Y = Y_0$,

$\mu = a_1 / 2 \neq 0,\ a_2 = -a_1^2 / 4$ the right circular cone $\sqrt{3I_2^{'}} = Y_0 - \mu I_1$ of Drucker and Prager is retrieved. Furthermore $a_1 = 0,\ a_2 \neq 0$ establishes Green's ellipsoid, Grren (1972).

2. The stress-like internal variable $R(e_v)$ of Equation 5.4 plays the role of a hardening function dependent on the strain-like internal e_v defined in the next section.

Additionally a plastic potential Φ^* is introduced with the same mathematical structure as the overstress function defined in Equation5:

$$
\begin{aligned}
&1. \quad \Phi^* &&= I_2^{'} - \frac{1}{3}\varphi^* \\
&2. \quad \varphi^* &&= Y^2 - a_1^* Y_0 I_1 - a_2^* I_1^2
\end{aligned}
\tag{6}
$$

Compared to the overstress function Φ additional material parameters related to the plastic potential Φ^* are a_1^*, a_2^*.

2.3 Rate equations

For evolution of the plastic strain tensor the following rate equation is derived from the plastic potential as

$$
\begin{aligned}
&1. \quad \dot{\boldsymbol{\varepsilon}}_{pl} &&= \dot{\lambda}\frac{\partial \Phi^*}{\partial \boldsymbol{\sigma}} = \dot{\lambda}\boldsymbol{\sigma}_{dev} + \dot{\lambda} t \mathbf{1} \\
&2. \quad t &&= \frac{1}{3}(a_1^* Y_0 + 2a_2^* I_1)
\end{aligned}
\tag{7}
$$

Here the plastic multiplier is postulated as a Perzny type parameter

$$
\dot{\lambda} = \left(\frac{< \Phi >}{K} \right)^n , \tag{8}
$$

and where the brackets mean $< x >= x$ for $x > 0, < x >= 0$ for $x \leq 0$. Consequently the plastic multiplier $\dot{\lambda}$ is always non-negative. In order to formulate a rate equation for the strain like internal variable e_v two different approaches are considered: For both cases the following equivalence of dissipated power expressions are postulated

$$
\begin{array}{llllll}
Case\,1. & \dot{e}Y & = & \boldsymbol{\sigma}:\dot{\boldsymbol{\varepsilon}}^{pl} & \Rightarrow & \dot{e} = \dfrac{1}{Y}\boldsymbol{\sigma}:\dot{\boldsymbol{\varepsilon}}^{pl} = \dfrac{\dot{\lambda}}{Y}\left(tI_1 + 2I_2^{'}\right) \\
Case\,2. & \dot{e}Y_0 & = & \boldsymbol{\sigma}:\dot{\boldsymbol{\varepsilon}}^{pl} & \Rightarrow & \dot{e} = \dfrac{1}{Y_0}\boldsymbol{\sigma}:\dot{\boldsymbol{\varepsilon}}^{pl} = \dfrac{\dot{\lambda}}{Y_0}\left(tI_1 + 2I_2^{'}\right)
\end{array}
\tag{9}
$$

2.4 Thermodynamic consistency

A thermodynamic argument requires the dissipation for arbitrary stress and strain states to be non-negative, see e.g. Truesdell and Noll (1965). Without going into details of the thermodynamic framework the (reduced) dissipation as a consequence of the inelastic strain rate (7) is calculated according to $D \;=\; \boldsymbol{\sigma}:\dot{\boldsymbol{\varepsilon}}_{pl} - R\dot{e}_v \;\geq\; 0$. Upon considering Case 1 and Case 2 in Equation 9 the following relations are obtained

$$
\begin{array}{lllll}
Case\,1. & D = (Y - R)\dot{e} & = & Y_0\dot{e} & \geq o \\
Case\,2. & D = (Y_0 - R)\dot{e} & & & \geq 0
\end{array}
\tag{10}
$$

Since Y_0 is always non-negative, the requirement for Case 1 in Equation 10 is equivalent to the following inequality

$$
\begin{aligned}
\boldsymbol{\sigma}:\dot{\boldsymbol{\varepsilon}}_{pl} &= \dot{\lambda}\boldsymbol{\sigma}:\left(\boldsymbol{\sigma}_{dev} + t\mathbf{1}\right) \\
&= \dot{\lambda}\boldsymbol{\sigma}:\boldsymbol{\sigma}_{dev} + \frac{\dot{\lambda}}{3}\boldsymbol{\sigma}:\mathbf{1}\,a_1^{*}Y_0 + \frac{\dot{\lambda}}{3}\boldsymbol{\sigma}:\mathbf{1}\;2a_2^{*}I_1 \\
&= 2\dot{\lambda}\,I_2^{'} + \frac{\dot{\lambda}}{3}I_1\,a_1^{*}Y_0 + \frac{2\dot{\lambda}}{3}a_2^{*}I_1^{2} \\
&\geq 0
\end{aligned}
$$

In the above derivations additionally Equation 4 for the first stress invariant I_1 and the second deviatoric stress invariant $I_2^{'}$ has been used. Several conclusions can be envisaged in order to satisfy the above inequality. Since, due to Equation8 the plastic multiplier $\dot{\lambda}$ and, furthermore, $I_2^{'}$ and I_1^{2} are always non-negative, we choose the restrictions $a_1^{*} = 0, \quad a_2^{*} \geq 0$ on the material parameters thus satisfying inequality 10 for all stress and strain states.

Concerning Case 2 of the inequality 10 additionally the term $(Y_0 - R)$ must be non-negative. For the specific hardening function of Equation 5.4 with $Y_0, H, q \geq 0$ this is satisfied by the restriction $\dot{e}_v \leq (Y_0 - q)/H$. To summarise, the following restrictions on the material parameters and the strain-like internal variable $\dot{e}_v$ are sufficient for thermodynamic consistency of the constitutive equations

$$\begin{array}{llllll} Case\,1. & Y_0 \geq 0, & a_1^* = 0, & a_2^* \geq 0, & & \\ Case\,2. & Y_0 \geq 0, & a_1^* = 0 & a_2^* \geq 0, & H \geq 0 \quad q \geq 0 & e_v \leq \dfrac{Y_0 - q}{H} \end{array} \tag{11}$$

3. Numerical implementation for rate dependent plasticity

3.1 Integration scheme for the evolution equations

Following standard integration procedures in finite element techniques a *strain-driven* algorithm is considered, where the total strain tensor ${}^{(n+1)}\boldsymbol{\varepsilon}$ and initial values ${}^{(n)}\boldsymbol{\varepsilon}_{pl}$, ${}^{(n)}e_v$ are given at a representative time step ${}^{(n)}t$. Then, it is the object to find the corresponding quantities ${}^{(n+1)}\boldsymbol{\varepsilon}_{pl}$, ${}^{(n+1)}e_v$ at time ${}^{(n+1)}t = {}^{(n+1)}t + \Delta t$ consistent with the constitutive equations of the previous sections, see e.g. Simo and Hughes (1998).

For numerical integration of the rate equations 7, 8 and 9 an Euler backward rule renders the following update scheme for the plastic strain tensor

$$\begin{array}{llll} 1. & {}^{(n+1)}\boldsymbol{\varepsilon}^{pl} & = & {}^{(n)}\boldsymbol{\varepsilon}^{pl} + \Delta\boldsymbol{\varepsilon}^{pl} \\ 2. & \Delta\boldsymbol{\varepsilon}^{pl} & = & \Delta\lambda\ {}^{(n+1)}\boldsymbol{\sigma}_{dev} + \Delta\lambda\ {}^{(n+1)}t\,\mathbf{1} \\ 3. & {}^{(n+1)}t & = & \dfrac{1}{3}(a_1^*\ Y_0 + 2a_2^*\ {}^{(n+1)}I_1) \\ 4. & \Delta\lambda & = & \Delta t\left(\dfrac{<\Phi>}{K}\right)^n \end{array} \tag{12}$$

and the strain like internal variable.

$$
\begin{aligned}
&1. \quad {}^{(n+1)}e_v = {}^{(n)}e_v + \Delta e_v \\
&2. \quad \Delta e_v = \begin{cases} \dfrac{\Delta\lambda}{Y}\left({}^{(n+1)}t\ {}^{(n+1)}I_1 + 2\ {}^{(n+1)}I_2^{'}\right) & \text{for Case 1} \\ \dfrac{\Delta\lambda}{Y_0}\left({}^{(n+1)}t\ {}^{(n+1)}I_1 + 2\ {}^{(n+1)}I_2^{'}\right) & \text{for Case 2} \end{cases}
\end{aligned}
\tag{13}
$$

respectively, and where Case 1 and Case 2 refer to the distinction introduced in Equation 10. In order to simplify the notation, the index $n+1$ referring to the actual time step will be omitted subsequently.

3.2 Volumetric/deviatoric split of the integration scheme

The integration scheme (12) can written in terms of the volumetric and deviatoric stress tensor as follows: Upon inserting Equation 12.1 into Equation3.1, solving for $\boldsymbol{\varepsilon}^{el}$ and inserting into Equation3.2 renders

$$
\boldsymbol{\sigma} = \boldsymbol{\sigma}^{tr} - \mathbf{C} : \Delta\boldsymbol{\varepsilon}^{pl}, \quad \textit{where} \quad \boldsymbol{\sigma}^{tr} = \mathbf{C} : (\boldsymbol{\varepsilon} - {}^{(n)}\boldsymbol{\varepsilon}^{pl}) \tag{14}
$$

Furthermore, using the relation

$$
\mathbf{C} : \Delta\boldsymbol{\varepsilon}^{pl} = 2G\,\Delta\lambda\boldsymbol{\sigma}_{dev} + \Delta\lambda\,3t\,K\,1 \tag{15}
$$

the deviatoric/volumetric split of Equation14 is obtained as

$$
\begin{aligned}
&1. \quad \boldsymbol{\sigma}_{vol} = \boldsymbol{\sigma}_{vol}^{tr} - K\Delta\lambda\,3t\,1, \quad \boldsymbol{\sigma}_{vol}^{tr} = \frac{1}{3}I_1^{tr}\,1, \quad I_1^{tr} = 3K\,tr[\boldsymbol{\varepsilon} - {}^{(n)}\boldsymbol{\varepsilon}^{pl}] \\
&2. \quad \boldsymbol{\sigma}_{dev} = \boldsymbol{\sigma}_{dev}^{tr} - 2G\Delta\lambda\boldsymbol{\sigma}_{dev}, \quad \boldsymbol{\sigma}_{dev}^{tr} = 2G(\boldsymbol{\varepsilon}_{dev} - {}^{(n)}\boldsymbol{\varepsilon}_{dev}^{pl})
\end{aligned}
\tag{16}
$$

and where $tr[\boldsymbol{\varepsilon} - {}^{(n)}\boldsymbol{\varepsilon}^{pl}] = \mathbf{1} : (\boldsymbol{\varepsilon} - {}^{(n)}\boldsymbol{\varepsilon}^{pl})$. Note, that the trial stress tensors $\boldsymbol{\sigma}_{dev}^{tr}$ and $\boldsymbol{\sigma}_{vol}^{tr}$ are determined directly from the given quantities ${}^{(n+1)}\boldsymbol{\varepsilon}$ and ${}^{(n)}\boldsymbol{\varepsilon}_{pl}$, however, the final stress tensors $\boldsymbol{\sigma}_{dev}$ and $\boldsymbol{\sigma}_{vol}$ are obtained iteratively as discussed next.

3.3 Reduction of the integration scheme to a single scalar equation for Case 2

In the following it will be shown, that Equation 16 can be reduced to a single scalar equation, analogously to the radial-return scheme of elasto plasticity described e.g. in Simo and Hughes (1998). For reasons explained below, we will concentrate on Case 2 introduced in Equation10.

Inserting Equation12 into Equation16.1 implies the scalar equation

$$\frac{1}{3}I_1 = \frac{1}{3}I_1^{tr} - K\,\Delta\lambda\,3t = \frac{1}{3}I_1^{tr} - K\,\Delta\lambda\,(a_1^* Y_0 + 2a_2^*\,I_1)\,,$$

which can be solved for I_1 as

$$I_1 = \frac{I_1^{tr} - 3K\,\Delta\lambda\,a_1^*\,Y_0}{1 + 3K\;\Delta\lambda\;2a_2^*}\,. \tag{17}$$

Upon rewriting Equation16.2 yields

$$\delta\,\boldsymbol{\sigma}_{dev} = \boldsymbol{\sigma}_{dev}^{tr}, \quad where \quad \delta = (1 + 2G\Delta\lambda)\,, \tag{18}$$

which means, that $\boldsymbol{\sigma}_{dev}$ is coaxial to $\boldsymbol{\sigma}_{dev}^{tr}$. Taking the inner product of both sides in Equation18 renders

$$\delta^2\,\boldsymbol{\sigma}_{dev} : \boldsymbol{\sigma}_{dev} = \boldsymbol{\sigma}_{dev}^{tr} : \boldsymbol{\sigma}_{dev}^{tr} \quad \Rightarrow \quad \delta^2 I_2^{'} = I_2^{'tr}\,, \tag{19}$$

where analogously to Equation(4) the second invariant of the deviatoric trial stress tensor $I_2^{'tr}$ = $1/2\;\; \boldsymbol{\sigma}_{dev}^{tr} : \boldsymbol{\sigma}_{dev}^{tr}$ has been introduced.

By use of Equation12.2 and Equation19 the strain like internal variable of Equation13.1 can now explicitly be written as

$$e_v = {}^{(n)}e_v + \frac{\Delta\lambda}{Y_0}\left(t\,I_1 + \frac{2}{\delta^2}\,I_2^{'tr} \right). \tag{20}$$

Note, that this explicit formulation is not possible for Case 1 introduced in Equation10, since, according to Equation5 the hardening variable $Y = Y[e_v]$ is dependent on the strain like variable e_v .

Next, upon reformulating Equation12.4 and furthermore Equation5.1 it follows $\Phi =$ $I_2^{'} - 1/3\,H = 0$ for the case of loading, which allows the following nonlinear residual of Equation19 in terms of the plastic multiplier

$$
\begin{array}{llll}
1. & r[\Delta\lambda] & = & 3I_2^{'tr} - \varphi\delta^2 - \left(\dfrac{\Delta\lambda}{\Delta t}\right)^{\frac{1}{n}} K \quad where \\
2. & \varphi & = & Y^2 - a_1 Y_0 I_1 - a_2 I_1^2 \\
3. & I_1 & = & \dfrac{I_1^{tr} - 3K\,\Delta\lambda\, a_1^* Y_0}{1 + 3K\,\Delta\lambda\, 2a_2^*} \\
4. & \delta & = & 1 + 2G\,\Delta\lambda \\
5. & Y & = & Y_0 + R \\
6. & R & = & q(1 - \exp[-be_v]) + He_v \\
7. & e_v & = & {}^{(n)}e_v + \dfrac{\Delta\lambda}{Y_0}\left(t\;\; I_1 + \dfrac{2}{\delta^2}\;\; I_2^{'tr}\right)
\end{array}
\tag{21}
$$

The above nonlinear equation is solved iteratively with a Newton method

$$
\Delta\lambda^{(k+1)} = \Delta\lambda^{(k)} - \frac{1}{J^{(k)}} r[\Delta\lambda^{(k)}], \quad k = 0,1,2,...., \text{ where.} \quad J = \frac{\partial\, r}{\partial\, \Delta\lambda} \tag{22}
$$

From the Equations 21 the following result is obtained for J :

$$
\begin{array}{llll}
1. & J & = & -1\left(\delta^2 \dfrac{\partial\varphi}{\partial\Delta\lambda} + 2\varphi\delta 2G\right) - \dfrac{1}{n}\left(\dfrac{\Delta\lambda}{\Delta t}\right)^{\frac{1}{n}-1} K \dfrac{1}{\Delta t}, \quad \text{where} \\
2. & \dfrac{\partial\varphi}{\partial\Delta\lambda} & = & 2YY' \dfrac{\partial\Delta e}{\partial\Delta\lambda} - (a_1 Y_0 + 2a_2 I_1) \dfrac{\partial I_1}{\partial\Delta\lambda} \\
3. & \dfrac{\partial I_1}{\partial\Delta\lambda} & = & -3K \dfrac{I_1\, 2a_2^* + a_1^* Y_0}{1 + 3K\,\Delta\lambda\, 2a_2^*} \\
4. & \dfrac{\partial\Delta e}{\partial\Delta\lambda} & = & \dfrac{1}{Y_0}\left(t\;\; I_1 + \dfrac{2}{\delta^2}\;\; I_2^{'tr}\right) + \dfrac{\Delta\lambda}{Y_0}\left(\dfrac{2a_2^*}{3}\dfrac{\partial I_1}{\partial\Delta\lambda} I_1 + t\dfrac{\partial I_1}{\partial\Delta\lambda} - \dfrac{8G}{\delta^3}\;\; I_2^{'tr}\right)
\end{array}
\tag{23}
$$

Note, that additionally the notation $Y' = dY / de_v$ has been used.

3.4 Final stress and strain determination

After having determined the plastic multiplier $\Delta\lambda$ the final stress tensor is obtained as

$$\boldsymbol{\sigma} = \boldsymbol{\sigma}_{dev} + \boldsymbol{\sigma}_{vol}\text{, where } \boldsymbol{\sigma}_{dev} = \frac{1}{\delta}\boldsymbol{\sigma}^{tr}_{dev}, \quad \boldsymbol{\sigma}_{vol} = \frac{1}{3} I_1 \, \mathbf{1}, \tag{24}$$

and the plastic strains are updated according to the Equations (11) and (13), respectively.

3.5 Algorithmic tangent modulus

The algorithmic tangent modulus necessary for applying a Newton method for iterative solution of the global equilibrium problem requires the derivative of the stress tensor $\boldsymbol{\sigma}$ defined in Equation24 with respect to the total strain tensor $\boldsymbol{\varepsilon}$, i.e.

$$\mathbf{C} = \frac{d\boldsymbol{\sigma}}{d\boldsymbol{\varepsilon}}. \tag{25}$$

Straightforward differentiation renders the following result

$$\mathbf{C} = \frac{2G}{\delta}\mathbf{I}_{dev} + \left(\frac{1}{3}\frac{\partial I_1}{\partial \Delta\lambda}\mathbf{1} - \frac{2G}{\delta^2}\boldsymbol{\sigma}^{tr}_{dev} \right) \otimes \frac{\partial \Delta\lambda}{\partial \boldsymbol{\varepsilon}} + \frac{B}{1 + 3K\,\Delta\lambda\, 2a_2^*}\mathbf{1} \otimes \mathbf{1}, \tag{26}$$

and where $\partial I_1 / \partial \Delta\lambda$ is given in Equation 23.3. The term $\partial\Delta\lambda / \partial\boldsymbol{\varepsilon}$ is obtained as follows: we consider the local problem Equation 21 as an implicit function and conclude

$$r[\boldsymbol{\varepsilon}, \boldsymbol{\varepsilon}[\Delta\lambda]] = 0 \quad \Rightarrow \quad \frac{d\,r}{d\,\boldsymbol{\varepsilon}} = \frac{\partial r}{\partial \boldsymbol{\varepsilon}} + \frac{\partial r}{\partial \Delta\lambda}\frac{\partial \Delta\lambda}{\partial \boldsymbol{\varepsilon}} \quad \Rightarrow \quad \frac{\partial \Delta\lambda}{\partial \boldsymbol{\varepsilon}} = -J^{-1}\frac{\partial r}{\partial \boldsymbol{\varepsilon}}, \tag{27}$$

where J is already defined in Equation22. The result for $\partial r / \partial \boldsymbol{\varepsilon}$ is as follows

$$\frac{\partial r}{\partial \boldsymbol{\varepsilon}} = \left(a_1 Y_0 + 2a_2 I_1 - 2Y\,Y'\Delta\lambda\, t\frac{1}{Y_0} \right)\frac{\delta^2 3K}{1 + 3K\,\Delta\lambda\, 2a_2^*}\mathbf{1} + \left(3 - \frac{4Y\,Y'\Delta\lambda}{Y_0\delta^2} \right) 2G\boldsymbol{\sigma}^{tr}_{dev}. \tag{28}$$

The above results for the stress tensor Equation24, the plastic strains Equation12 and Equation 13 and the algorithmic tangent operator can be implemented into a general finite element program. The results shown below for the double U-specimen have been obtained with the program ABAQUS.

3.6 Simulation of rate dependent behaviour in axial and shear loading

The first example intends to verify the rate dependent formulation. To this end we use data from the literature documented in Disse (2004) for the adhesive material EP208. Here rate dependent experiments are obtained for both axial and shear loading. In this way additionally the SD-effect is activated for the simulation. The strain rate range for tension is $0.001 - 156\ \sec^{-1}$, for shear it is $0.001 - 435\ \sec^{-1}$. For simulation of the experimental effects material parameters $Y_0\ , q, b,$ $a_1\ , a_2\ , a_1^*, a_2^*, K, n$ introduced in Section 2 have to be determined. Furthermore the restriction $a_1^* = 0$ in Equation11 is taken into account. Several strategies can be envisaged for the task of parameter identification, see e.g. Mahnken (2004). For the problem at hand a non-linear least-squares functional is formulated considering the experimental data of. Then a Simplex Nelder algorithm is used for minimisation, see e.g. Press *et. al*.(1992). The resulting parameter set is summarized in Table 1.

Table 1. Material parameters for EP208 obtained from least-squares minimization

E [MPa]	ν [-]	Y_0 [MPa]	q [MPa]	b [-]	H [MPa]	a_1 [-]	a_2 [-]	a_1^* [-]	a_2^* [-]	K [-]	n [-]
1588.7	0.34	35.11	8.04	18.4	14.2	0.643	0.0	0.0	.352	10.7	3.48

The comparison of experiment and simulation for both axial loading and shear loading is depicted in Figure 1. The results demonstrate the capability of the model to simulate the strength difference including the hardening behaviour for the different loading cases with accuracy sufficient for practical purposes.

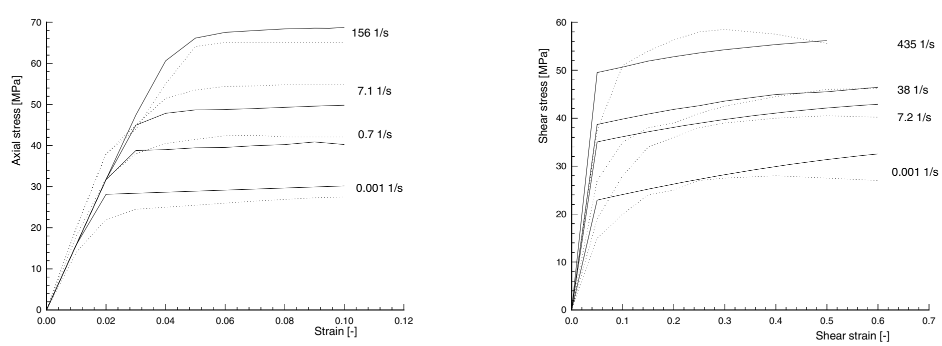

Figure 2: Comparison of simulation (solid line) and experiment (dotted line) for different strain rates, left: axial stress versus axial strain, right: shear stress versus shear strain

4. Extension to softening behavior

In order to simulate rate dependent material behaviour coupled to softening, the concept of effective stresses is included into the constitutive equations of Section 2. To this end the overstress function of Equation 5 is extended as follows:

$$\begin{array}{lll} 1. \quad \Phi & = & I'_{2,eff} - \frac{1}{3}\varphi \\ 2. \quad \varphi & = & Y^2 - a_1 Y_0 \, I_{1,eff} - a_2 I_{1,eff}^2 \\ 3. \quad Y & = & Y_0 + R[e_v] \\ 4. \quad R[e_v] & = & q(1-\exp[-be_v]) + He_v . \end{array} \tag{29}$$

Here additionally we defined the effective stress invariants

$$I_{1,eff} = \frac{I_1}{W}, \qquad I'_{2,eff} = \frac{I'_2}{W^2}, \tag{30}$$

where $W = W[e_v]$ is a damage function in terms of the inelastic strain explained in the ensuing section.

Different concepts are known from the literature for simulation of softening. Two well known approaches are published in Gurson (1977) and Lemaitre (1996). The first approach activates softening under a pure volumetric stress mode, thus rendering the material undamaged for a stress mode in shear. The second approach activates softening under a pure stress mode in shear, thus rendering the material undamaged for a volumetric stress mode. Both approaches have in common, that additional evolution equations are introduced for softening representation. In the following we propose a simple approach which accounts for both, softening evolution subject to deviatoric and volumetric stress states.

To this end a softening function is split multiplicatively as

$$W = W^{vol} \cdot W^{dev} . \tag{31.1}$$

For the deviatoric part we postulate

$$W^{dev} = \begin{cases} 1 & if \;\; e_v^{dev} \le e^{dev} \\ \exp(w^{*dev}(e_v^{dev} - e^{dev})^{n^{dev}}) & if \;\; e_v^{dev} > e^{dev} \end{cases}, \tag{31.2}$$

where e^{def} is a threshold value and n^{def} is an exponent. Using the additional material parameters w^{def} and d^{def} an additional scalar value is introduced as

$$w^{*dev} = \begin{cases} \dfrac{e_f^{dev} - e^{dev}}{d^{dev}} w^{dev} & if \;\; e_v^{dev} \le e^{dev} + d^{dev} \\ w^{dev} & if \;\; e_v^{dev} > e^{dev} + d^{dev} \end{cases} \tag{31.3}$$

Analogously, volumetric softening is introduced as

$$W^{vol} = \begin{cases} 1 & if \;\; e_v^{vol} \le e^{vol} \\ \exp(w^{*vol}(e_v^{vol} - e^{vol})^{n^{vol}}) & if \;\; e_v^{vol} > e^{vol}, \end{cases} \tag{31.4}$$

where

$$w^{*vol} = \begin{cases} \dfrac{e_f^{vol} - e^{vol}}{d^{vol}} w^{vol} & if \;\; e_v^{vol} \le e^{vol} + d^{vol} \\ w^{vol} & if \;\; e_v^{vol} > e^{vol} + d^{vol} \end{cases}, \tag{31.5}$$

and where e^{vol} is a threshold value, n^{vol} is an exponent, and w^{vol} and d^{vol} are additional material parameters. In this way, in Equation 9.3 and Equation 9.5 we have introduced the intervals $e^{vol} < e_v < e^{vol} + d^{vol}$ and $e^{dev} < e_v < e^{dev} + d^{dev}$ with individual scalars w^{*dev} and w^{*vol}, which gives the evolution of softening some more flexibility. The numerical implementation of these equations and a more elaborated dependence of some material parameters will be described in a later publication.

4.1 Axial and shear loading for a double U-shape specimen

In this example the constitutive relations, Equation 29 – Equation 31 are used to simulate the failure analysis of adhesively bonded joint in a double U-shape specimen. The geometry of the specimen is shown in Figure 2. It consists of two U-shape parts made out of steel with Young's modulus E = 210 GPa and Poission ratio $\nu = 0.3$, respectively. These are glued with the adhesive material BETAMATE 1496 with a thickness of d=0.3 mm. The specimen is subjected to two different loading cases: axial loading and shear loading. The actual loading is applied to the traverse of the experimental setup.

The right part of Figure 2 shows the finite element mesh. Shell elements are applied for the U-shape parts, and adhesive ABAQUS elements COH3D8 combined with a UMAT subroutine are used for the adhesive zone. The length of the interface elements is approximately 1 *mm* with a height of 0.3 *mm*, which corresponds to the thickness of the adhesive layer.

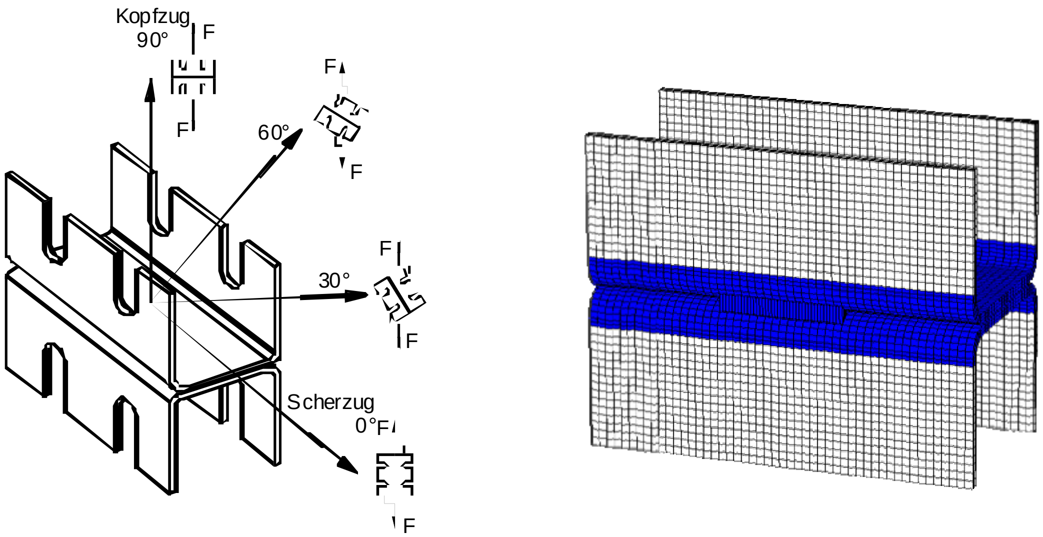

Figure 3: Double U-shape-specimen: Left, geometry and loading angles, see e.g. Hahn *et.al* (1996), Right, finite element discretisation with deformable regions (dark coulor) and rigid regions (white colour)

The material parameters for the constitutive equations are obtained on the basis of experimental data for BETAMATE 1496 taking into account the SD-effect, rate dependency and softening effects. As in the previous section a non-linear least-squares functional is minimized using a Simplex Nelder algorithm. Due to confidential agreements, the resulting material parameter set is not shown in this publication.

In the left part of Figure 3 and Figure 4 the resulting displacement-time curve locally near the adhesive layer are shown. These values are applied in the finite element simulation as loading conditions. Due to confidential reasons, units are not given in the diagrams. The right parts of Figure 3 and Figure 4 depict the resulting reaction forces of both load cases. It can be seen, that the experimental results are matched with an accuracy sufficient for practical purposes to predict the failure of the adhesively bonded joint in the U-shape specimen.

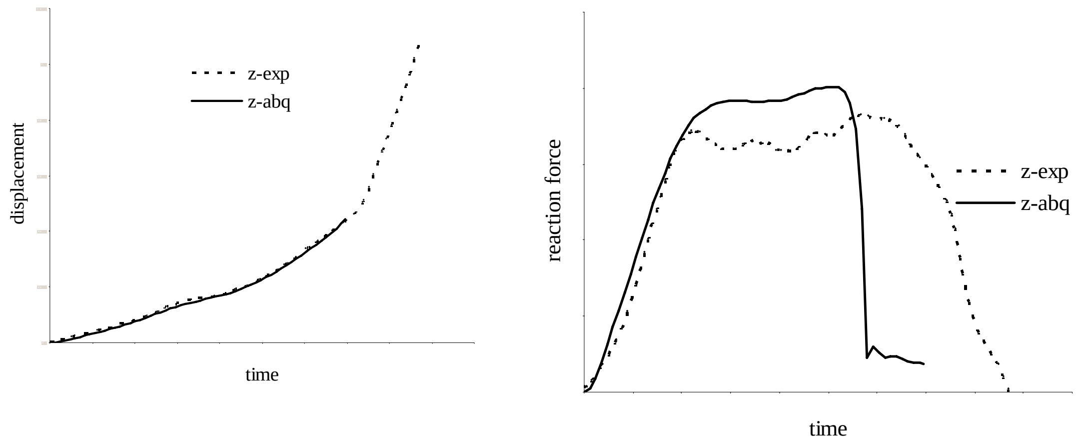

Figure 5. Double-U-Shape specimen in tension: (Left) Displacement-time curve locally near the adhesive layer. (Right) Corresponding load-displacement curves. Solid line refer to simulation and dotted line refer to experiment.

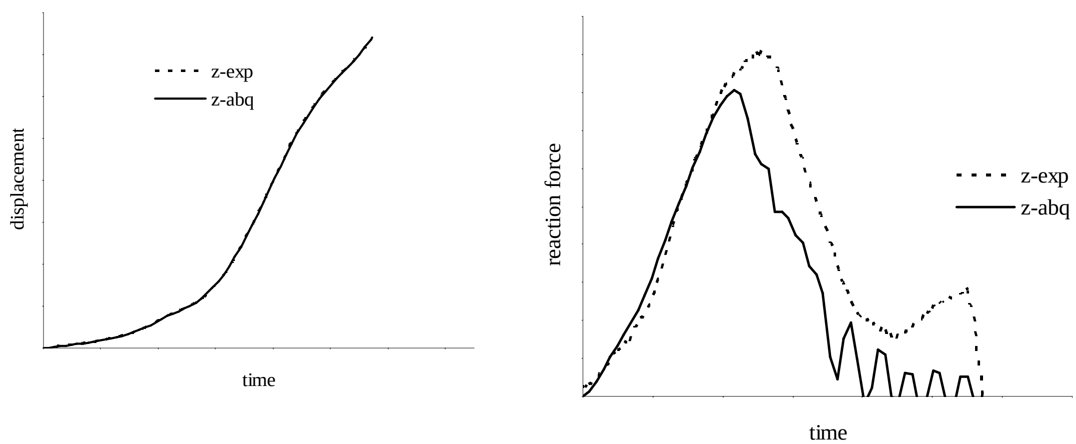

Figure 5. Double-U-Shape specimen in shear: (Left) Displacement-time curve locally near the adhesive layer. (Right) Corresponding load-displacement curves. Solid line refer simulation and dotted line refer to experiment.

5. Summary

This publication is concentrated on the simulation of so-called crash optimized adhesives, which exhibit the following experimental characteristics

1. A hardening regime with a strength difference effect.
2. Rate dependency
3. A softening regime

An implicit Euler backward scheme is described in detail for integration of the evolution equations for the case of rate dependency. The reduction to a one dimensional problem is done, which is solved with a Newton algorithm. Furthermore the associated algorithmic tangent operator for the global FE-equilibrium iteration scheme is derived. The comparison of calculated and experimental results demonstrates the capability of the model to simulate the related characteristic for the adhesive material EP208 of strength difference and rate dependency. Furthermore, the constitutive equations of rate dependency are extended to represent softening behavior. In a second example the constitutive equations are applied to investigate the failure of an adhesively bonded joint in a double-U-shape specimen made of the material BETAMATE 1496.Aspects for future work are the extension of the presented constitutive equations to large strain behavior, see e.g. Lion (2000), Govindjee and Reese (1997), Mahnken (2005)

6. Acknowledgement

Parts of the results in this paper are from the project P 676/13200/S24/10096/04, performed by Institut für Werkstofftechnik (IfW) Universität Kassel, Institut für Mechanik (IfM) Universität Kassel, Laboratorium für Werkstoff- und Fügetechnik (LWF), Universität Paderborn, IFS-Institut für Füge- und Schweißtechnik, TU Braunschweig, Fraunhofer Institut für Fertigungstechnik (IFAM), Bremen, Fraunhofer Institut Werkstoffmechanik (IWM), Freiburg, Fraunhofer Institut für Kurzzeitdynamik (EMI), Freiburg, Lehrstuhl für Technische Mechanik, Universität Paderborn, and with financial support by Forschungsvereinigung Stahlanwendung e.V., Düsseldorf, with resources of the Stiftung Stahlanwendungsforschung, Essen.

7. References

1. Altenbach, H.; Altenbach, J.; Zolochevsky, A., “Erweiterte Deformationsmodelle und Versagenskriterien der Werkstoffmechanik“, Deutscher Verlag für Grundstoffindustrie, Stuttgart, 1995

2. Betten, J.: Sklepus, S.; Zolochevsky, A., “A creep damage model for initially isotropic materials with dif-ferent properties in tension and compression”, Eng. Fract. Mechs., Vol 59, No 5 623-641, 1998

3. Disse, T.; “Untersuchungen zum geschwindigkeitsabhängigen Festigkeits- und Verformungsverhalten von Klebverbindungen”, Dissertation, University of Paderborn, 2004

4. Dean, G.; Crocker, L.; Read, B., Wright, L., “Prediction of deformation and failure of rubber-toughened adhesive joints”, Int. J. Adhesion & Adhesives, 24 (2004) 295-306

5. Duncan, B., Dean, G., “Measurements and models for design with modern adhesives”, Int. J. Adhesion & Adhesives, 23 (2004) 141-149
6. Ehlers, W., ”A single-surface yield function for geomaterials”, Archive of Applied Mechanics, 65 (1995) 246-259
7. Govindjee, S.; Reese, S., “A presentation and comparison of two large deformation viscoelasticity models”, ASME J. Eng. Mat. Tech., 119:251-255, 1997
8. Green, R.J., “A plasticity theory for porous solids”, Int. J. Mech. Sci., 14, (1972) 215-224
9. Gurson, A.L., “Continuum theory of ductile rupture by void nucleation and growth - I. Yield criteria and flow rules for porous ductile media”, Engng. Materials Technol., 99, 2-15 (1977)
10. Hahn, O.; Gieske, D.; Rhode, A.: Patentschrift DE 195 22 247 A1, Probe und Probenspannvorrichtung zum Einsatz in Zugmaschinen, 1996
11. Lemaitre,J., “A course on damage mechanics”, 2nd. ed., Berlin, Springer 1996
12. Lion, A.: “Constitutive modelling in finite thermoviscoplasticity: A physical approach based on nonlinear rheological elements”, Int. J. Plast. 16, 469-494 (2000)
13. Mahnken, R., “Strength difference in compression and tension and pressure dependence of yielding in elasto-plasticity”, Comp. Meths. Appl. Mech. Eng., Vol. 90, 5057-5080 (2001)
14. Mahnken, R., “Identification of material parameters for constitutive equations”, Encyclopedia of Computational Mechanics, Vol.2, Eds. E. Stein, de Borst, Hughes, Wiley and Sons, Chichester (2004)
15. Mahnken, R., “Simulation of strength difference for adhesive materials in finite deformation elasto-plasticity”, Comp. Meths in Appl. Mech. Eng. 194 (2005), 4097-4114
16. Mahnken, R. Schlimmer, , M., Simulation of strength difference in elasto-plasticity for adhesive materials, Int. J. Num. Meths. Eng., Volume 63, Issue 10, 1461-1477, 2005
17. Press, W.H.; Teukolsky, S.A.; Vetterling, W.T.; Flannery, B.P., “Numerical Recipies in Fortran”, Cambridge University Press, 1992
18. Schlimmer, M., “Fließverhalten plastisch kompressibler Werkstoffe“, Dissertation, RWTH Aachen, 1974
19. Schlimmer, M.., “Grundlagen zur Berechnung des mechanischen Verhaltens von strukturellen Klebverbindun-gen des Fahrzeugbaus“. Proc. Mechanisches Fügen und Kleben, Ed. O. Hahn, 2003
20. Simo, J.C.; Hughes, T.J.R., “Computational Inelasticity, Interdisciplinary Applied Mathematics”, Vol. 7, Me-chanics and Materials, Springer—Verlag, 1998
21. C. Truesdell, W. Noll: “The Nonlinear Field Theories of Mechanics”, Sec. Edition, Springer-Verlag, Berlin, 1965
22. Zolochevskii, A.A., “Modification of the theory of plasticity of materials differently resistant to tension and compression for simple loading processes”, Soviet Applied Mechanics (transl. Prikladnaya Mekhanika), **24** (12), 1212-1217, 1989